Inorganic Chemistry

Article

pubs.acs.org/IC

Polynuclear and Polymeric Gadolinium Acetate Derivatives with Large Magnetocaloric Effect

Fu-Sheng Guo, Ji-Dong Leng, Jun-Liang Liu, Zhao-Sha Meng, and Ming-Liang Tong*

Key Laboratory of Bioinorganic and Synthetic Chemistry of Ministry of Education, State Key Laboratory of Optoelectronic Materials and Technologies, School of Chemistry and Chemical Engineering, Sun Yat-Sen University, Guangzhou 510275, P. R. China

Supporting Information

ABSTRACT: Two ferromagnetic μ-oxo$_{acetate}$-bridged gadolinium complexes $[Gd_2(OAc)_2(Ph_2acac)_4(MeOH)_2]$ (**1**) and $[Gd_4(OAc)_4(acac)_8(H_2O)_4]$ (**2**) and two polymeric Gd(III) chains $[Gd(OAc)_3(MeOH)]_n$ (**3**) and $[Gd(OAc)_3(H_2O)_{0.5}]_n$ (**4**) (Ph_2acacH = dibenzoylmethane; acacH = acetylacetone) are reported. The magnetic studies reveal that the tiny difference in the Gd−O−Gd angles (Gd···Gd distances) in these complexes cause different magnetic coupling. There exist ferromagnetic interactions in **1**−**3** due to the presence of the larger Gd−O−Gd angles (Gd···Gd distances), and antiferromagnetic interaction in **4** when the Gd−O−Gd angle is smaller. Four gadolinium acetate derivatives display large magnetocaloric effect (MCE). The higher magnetic density or the lower M_W/N_{Gd} ratio they have, the larger MCE they display. Complex **4** has the highest magnetic density and exhibits the largest MCE (47.7 J K^{-1} kg^{-1}). In addition, complex **3** has wider temperature and/or field scope of application in refrigeration due to the dominant ferromagnetic coupling. Moreover, the statistical thermodynamics on entropy was successfully applied to simulate the MCE values. The results are quite in agreement with those obtained from experimental data.

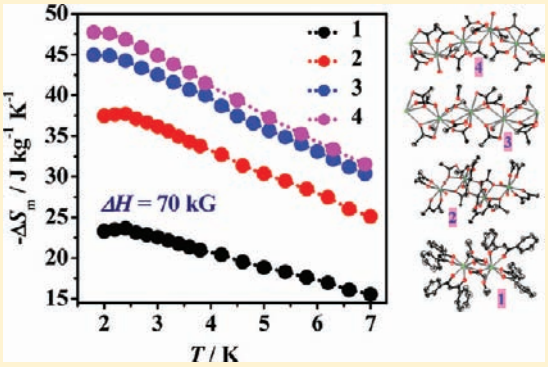

INTRODUCTION

The magnetocaloric effect (MCE) was discovered 130 ago and is defined as the adiabatic temperature change (the entropy change) of a magnetic material due to the application of a magnetic field.[1] This interesting phenomenon could be used in cooling applications via adiabatic demagnetization. Compared to vapor-cycle technology, magnetic refrigerators do not use ozone-depleting or global-warming volatile liquid refrigerants, which is an environmentally friendly alternate technology. Recent studies reveal that high-spin molecular nanomagnets[2−6] can exhibit larger MCE values than those found for lanthanide alloys and magnetic nanoparticles in the ultralow temperature region.[7] What is more, molecule-based magnets have more superiorities, for example: (1) weak intermolecular interaction can avoid the decrease of entropy change arising from long-range order; (2) they are convenient for studying mechanism; (3) they are prone to design, regulate and decorate reasonably.

Compared with the MCE reports on the 3d and 3d-4f family, few pure 4f cases have been documented.[8] However, a recent breakthrough was achieved in a well-known ferromagnetic dimeric gadolinium acetate tetrahydrate, $[Gd_2(OAc)_6(H_2O)_4]\cdot 4H_2O$,[4b] which has a large $-\Delta S_m$ value, more than 40 J K^{-1} kg^{-1}.

Theoretically, a well-performing magnetic refrigerant should possess the following factors: large spin ground state S, molecular isotropy, high spin degeneracy and a relatively small molecular mass. Then how does one obtain such a molecule? First, we should choose isotropic ions (such as Mn(II), Cu(II), HS-Fe(III), Gd(III)) and light ligands as far as possible. The magnetic entropy S_m is $R \ln(2Ns + 1)$, where the "Ns" is the total spin. So the high spin $Mn^{2+}(d^5)$, $Fe_{HS}^{3+}(d^5)$ and Gd^{3+} (f^7) are better choices. Second, the exchange interactions within Gd^{3+} (f^7) complexes are very weak as a result of the efficient shielding of the unpaired electrons in the 4f orbitals; S_m comes very close to the maximum entropy value per mole calculated as $NR \ln(2s + 1) = NR \ln 8$ (the paramagnetic molecule is assumed to have N noninteraction spins s). That will simplify matters; we just need to get the target molecule with high magnetic density (or low M_W/N_{Gd} ratio) and high spin degeneracy. Finally, compared with Mn^{2+} and HS-Fe^{3+}, "fatter" Gd^{3+} needs more ligands to cover itself, so, we can bring down the coordination number, or increase the dimension of the structure, to decrease the M_W/N_{Gd} ratio. Based on the above-mentioned conditions, pure gadolinium complexes catch our eye.

Herein we report two polynuclear Gd(III) complexes and two polymeric Gd(III) chains, namely, $[Gd_2(OAc)_2(Ph_2acac)_4(MeOH)_2]$ (**1**), $[Gd_4(OAc)_4(acac)_8(H_2O)_4]$ (**2**), $[Gd(OAc)_3(MeOH)]_n$ (**3**) and $[Gd(OAc)_3(H_2O)_{0.5}]_n$ (**4**) with M_W/N_{Gd} = 695 (**1**), 433 (**2**), 366 (**3**) and 343 (**4**). Magnetic studies reveal that the higher magnetic density or the lower M_W/N_{Gd} ratio they have in the gadolinium acetate family, the larger MCE they display.

Received: August 22, 2011
Published: December 6, 2011

   dx.doi.org/10.1021/ic2018314 | Inorg. Chem. 2012, 51, 405−413

Table 1. Crystallographic Data and Structural Refinement Summary for 1−4

complex	1	2	3	4
formula	$C_{66}H_{58}Gd_2O_{14}$	$C_{48}H_{76}Gd_4O_{28}$	$C_7H_{13}GdO_7$	$C_{12}H_{20}Gd_2O_{13}$
FW	1389.62	1730.09	366.42	686.78
temp, K	298(2)	298(2)	298(2)	298(2)
cryst syst	triclinic	triclinic	monoclinic	monoclinic
space group	$P\bar{1}$	$P\bar{1}$	$P2_1/c$	Cc
a (Å)	10.2572(7)	11.6327(3)	12.1092(5)	16.1147(12)
b (Å)	11.9092(9)	11.7971(4)	12.1790(4)	16.7364(9)
c (Å)	13.7512(8)	13.6862(3)	7.6817(3)	8.4586(5)
α (deg)	97.530(2)	106.643(1)	90	90
β (deg)	99.024(2)	113.051(1)	90.637(2)	116.194(2)
γ (deg)	112.257(2)	102.055(1)	90	90
V (Å)^3	1501.68(18)	1542.17(7)	1132.81(7)	2047.0(2)
Z	1	1	4	4
F(000)	694	844	700	1296
cryst size (mm)	0.13 × 0.09 × 0.06	0.10 × 0.07 × 0.04	0.03 × 0.09 × 0.12	0.03 × 0.04 × 0.07
ρ_{calcd} (g cm^{-3})	1.537	1.863	2.149	2.228
μ(Mo Kα) (mm^{-1})	2.254	4.326	5.867	6.482
θ range (deg)	3.25−25	3.11−26	3.14−27.47	3.62−27.48
reflns collected, R_{int}	11325, 0.0540	11876, 0.0208	6765, 0.0349	5660, 0.0538
indep reflns	5721	5944	2185	3571
R_1[a] ($I > 2\sigma(I)$)	0.0390	0.0247	0.0294	0.0424
wR_2[b] (all data)	0.0655	0.0552	0.0687	0.1179
GOF	1.135	1.042	1.091	1.144
Flack param				0.04(4)

[a] $R_1 = \sum||F_o| - |F_c||/\sum|F_o|$. [b] $wR_2 = [\sum w(F_o^2 - F_c^2)^2/\sum w(F_o^2)^2]^{1/2}$.

Complex **4** has the highest magnetic density and exhibits the largest MCE (47.7 J K^{-1} kg^{-1}) among the four gadolinium acetate derivatives, which is also highest among the recently reported MCE values.

EXPERIMENTAL SECTION

Materials and General Procedures. All of the chemicals were obtained from commercial sources and used without further purification. The IR spectra were recorded from KBr disks in the range 4000−400 cm^{-1} with a Bruker-tensor 27 spectrometer.

Synthesis. *$[Gd_2(OAc)_2(Ph_2acac)_4(MeOH)_2]$ (**1**).* Ph_2acacH (0.090 g, 0.4 mmol) was dissolved in 30 mL of MeOH followed by the addition of acetic acid (0.024 g, 0.4 mmol) to give a colorless solution. After about 5 min of stirring, $[Gd_2(OAc)_6(H_2O)_4]\cdot 4H_2O$ (0.163 g, 0.2 mmol) was added to the solution. It was then stirred for another 5 min and filtered. The filtrate was left undisturbed to give X-ray quality light yellow crystals of **1** (yield: 35%) in 2 to 3 h. Elemental analysis (%) calcd for $C_{66}H_{58}Gd_2O_{14}$: C 57.04, H 4.21. Found: C 56.96, H 4.24. Infrared (KBr disk) cm^{-1}: 1597 (s), 1551 (s), 1521 (s), 1479 (s), 1454 (s), 1441 (w), 1394 (s), 1313 (m), 1223 (w), 1180 (w), 1070 (w), 1024 (w), 761 (w), 722 (m), 689 (m), 610 (w).

*$[Gd_4(OAc)_4(acac)_8(H_2O)_4]$ (**2**).* A mixture of Hacac (0.200 g, 2.0 mmol) and triethylamine (0.200 g, 2.0 mmol) in methanol (15 mL) was refluxed for a half-hour, and $[Gd_2(OAc)_6(H_2O)_4]\cdot 4H_2O$ (0.404 g, 0.5 mmol) was added. The resulting solution was then stirred under reflux for three hours and filtered. Upon slow evaporation over 1 week the filtrate yielded X-ray quality colorless block crystals (yield: 18%). Elemental analysis (%) calcd for $C_{48}H_{76}Gd_4O_{28}$: C 33.32, H 4.43. Found: C 33.64, H 4.33. Infrared (KBr disk) cm^{-1}: 3399 (m), 1592 (s), 1522 (s), 1388 (s), 1266 (m), 1019 (m), 924 (m), 764 (w), 679 (m), 656 (m).

*$[Gd(OAc)_3(MeOH)]_n$ (**3**).* Hacac (0.030 g, 0.3 mmol) was dissolved in 25 mL of MeOH followed by the addition of $[Gd_2(OAc)_6(H_2O)_4]\cdot 4H_2O$ (0.122 g, 0.15 mmol) to give a colorless solution. After being stirred and heated for about 10 min, it was then filtered. The filtrate was left undisturbed to give X-ray quality colorless crystals of **3** (yield: 35%) in 2 days. Elemental analysis (%) calcd for $C_7H_{13}GdO_7$: C 22.94, H 3.57. Found: C 22.74, H 3.62. Infrared (KBr disk) cm^{-1}: 1544 (s), 1456 (s), 1420 (s), 1387 (s), 1314 (m), 1053 (w), 1024 (w), 967 (w), 945 (w), 684 (m).

*$[Gd(OAc)_3(H_2O)_{0.5}]_n$ (**4**).* $[Gd_2(OAc)_6(H_2O)_4]\cdot 4H_2O$ (0.122 g, 0.15 mmol) was added to MeCN−CH_2Cl_2 (v/v = 1:1, 15 mL). The resulting solution was resealed in a 25-mL Teflon-lined, stainless steel vessel and heated at 120 °C for 48 h, and then cooled at a rate of ca. 5 °C h^{-1}. Colorless crystals (yield: 30%) were obtained. Elemental analysis (%) calcd for $C_{12}H_{20}GdO_{13}$: C 20.99, H 2.94. Found: C 20.78, H 3.09. Infrared (KBr disk) cm^{-1}: 3395 (w), 1546 (s), 1455 (s), 1419 (s), 1388 (m), 1316 (m), 1054 (w), 1024 (w), 966 (w), 945 (w), 683 (m).

X-ray Structure Determination. Diffraction data for complexes **1**, **2**, **3** and **4** were recorded at 298(2) K on a Rigaku R-AXIS SPIDER Image Plate diffractometer with graphite-monochromated Mo Kα radiation (λ = 0.71073 Å). Data collection and processing (cell refinement, data reduction and absorption) were performed using the program *PROCESS-AUTO*. The structures were solved by direct methods, and all non-hydrogen atoms were refined anisotropically by least-squares on F^2 using the *SHELXTL* program. Hydrogen atoms on organic ligands were generated by the riding mode. A summary of the crystallographic data and refinement parameters is provided in Table 1. CCDC 828783 (**1**), CCDC 828785 (**2**), CCDC 838754 (**3**), and CCDC 838755 (**4**) contain the supplementary crystallographic data for this paper. These data can be obtained free of charge from the Cambridge Crystallographic Data Center via www.ccdc.cam.ac.uk/data_request/cif.

Magnetic Measurements. Magnetic susceptibility measurements were performed using a Quantum Design MPMS XL-7 SQUID magnetometer. Diamagnetism was estimated from Pascal constants.

RESULTS AND DISCUSSION

Synthesis. Complex **1** was initially isolated from the reaction of $Gd(OAc)_3\cdot 4H_2O$ with Ph_2acacH in the presence of triethylamine in MeOH. The microcrystals formed immediately upon stirring due to the poor solubility in MeOH, but the crystal quality is not good for X-ray

dx.doi.org/10.1021/ic2018314 | Inorg. Chem. 2012, 51, 405−413

crystallography. The presence of triethylamine would accelerate the reaction, so we later replaced triethylamine by acetic acid and obtained X-ray quality crystals in about 2 h.

We can improve the magnetic density to obtain one enhanced MCE complex, and one method is to use a small ligand. In complex **2**, the replacement of Ph_2acacH by Hacac fulfilled our plans. The crystals of **2** did not form as quickly as **1**, so heating and the presence of base (triethylamine) are essential. Our next goal was to investigate whether the change of auxiliary ligand would enforce further structural distortions and switch the magnetic behavior (ferromagnetic/antiferromagnetic).

Polymerization is another method to improve the magnetic density. Complex **3** was prepared via the 1:1 Hacac/$[Gd_2(OAc)_6(H_2O)_4]\cdot 4H_2O$ reaction mixture. According to the synthetic method reported by the literature,[9] the reaction needs more time to be heated and stirred than what we did. To make further improvement on the magnetic density, in complex **4**, we changed the synthesis conditions including the absence of MeOH.

Crystal Structures. The single-crystal X-ray structural analysis reveals that $[Gd_2(OAc)_2(Ph_2acac)_4(MeOH)_2]$ (**1**) crystallizes in the triclinic space group $P\bar{1}$ with a half formula unit in the asymmetric unit cell. **1** is a neutral dinuclear structure containing two Gd^{III}, two OAc^- and four Ph_2acac^- ligands as well as two methanol ligands (Figure 1a). The two symmetry-related Gd^{III} ions are linked by two single-atom O bridges from two μ-η^2:η^1 acetate ligands with Gd···Gd distance of 4.128(4) Å and Gd−O−Gd angle of 113.65(18)°. Each Gd^{III} ion is further coordinated by two Ph_2acac^- ligands and one monodentate MeOH ligand to complete the square-antiprismatic coordination geometry. Both Ph_2acac^- ligands are chelating, quite different from those found in $\{Ln_5(Ph_2acac)_{10}(OH)_5\}$.[10] The smallest intermolecular Gd···Gd separation is 9.719(7) Å. There exist intramolecular O−H···O hydrogen bonding interactions (O6···O2A = 2.715(6) Å, O6−H6···O2A = 164.7°).

Complex $[Gd_4(OAc)_4(acac)_8(H_2O)_4]$ (**2**) crystallizes in the triclinic space group $P\bar{1}$ with a half formula unit in the asymmetric unit cell. **2** is a neutral tetranuclear structure containing four coplanar Gd^{III} ions, four acetate groups in the μ-η^2:η^1 and μ_3-η^2:η^2 coordination modes, eight chelated $acac^-$ groups and four aqua ligands (Figure 1b,c).

The inner symmetry-related Gd2 and Gd2A ions are coordinated in nine-coordinate (capped square-antiprismatic) geometry, while the terminal Gd1 and Gd1A are in eight-coordinate (square-antiprismatic) geometries. All the adjacent Gd1···Gd2, Gd2···Gd2A, and Gd1A···Gd2A ion pairs are connected through two single-atom O bridges from the μ-η^2:η^1 and μ_3-η^2:η^2 acetato groups, respectively. Between Gd2 and Gd2A, the two inversion-related bridging atoms O4 and O4A are from the μ_3-η^2:η^2 acetato groups. The distance between Gd1 and Gd2 is 4.271(6) Å with Gd1−O1−Gd2 and Gd1−O3−Gd2 angles of 117.73(9) and 114.45(9)°, respectively. The Gd2···Gd2A distance is 4.334 Å, and the Gd2−O4/O4A−Gd2A angle is 117.13(8)°. The Gd1···Gd2A or Gd1A···Gd2 pair with the separation of 7.086(2) Å is bridged by anti-anti acetate group. All eight $acac^-$ groups only act as chelated ligands, quite different from those found in $\{Ln_4\}$ and $\{Ln_9\}$.[11] The shortest intermolecular Gd···Gd distance is 6.013(1) Å. Besides, there exist abundant intra- and intermolecular O−H···O hydrogen bonding interactions (Figure 1d).

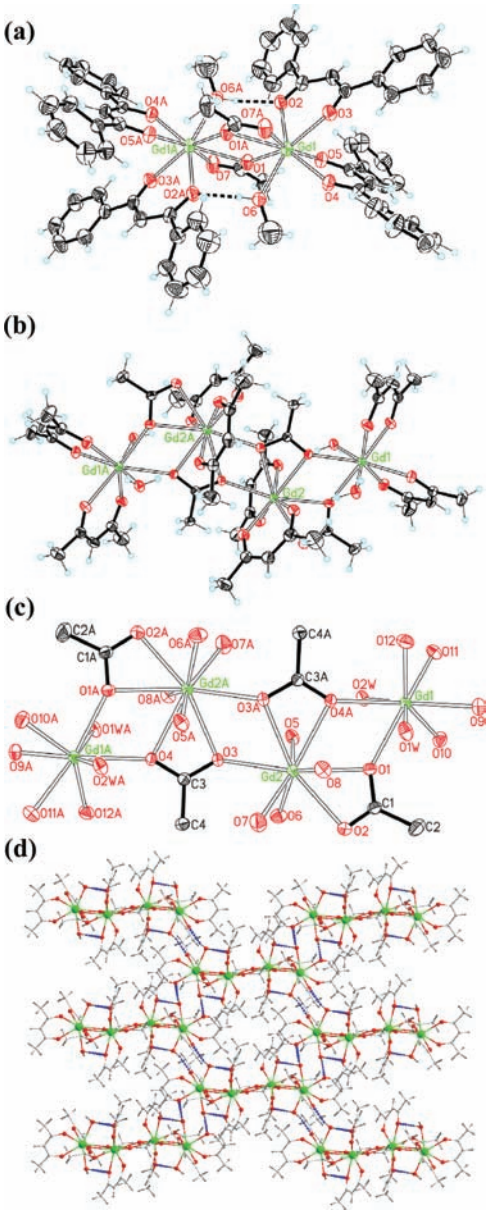

Figure 1. *ORTEP* plots of the molecular and core structures of **1** (a) and **2** (b, c) with ellipsoids at the 30% probability level. The 2D hydrogen-bonded layer for **2** (d). Symmetry codes: $-x + 1, -y + 1, -z + 1$ for **1** and $-x, -y, -z$ for **2**.

Different from those of **1** and **2**, **3** has a one-dimensional (1D) coordination chain structure (Figure 2a). Each Gd(III) ion in **3** is nine-coordinated in capped square-antiprism geometry. The adjacent Gd(III) ions are bridged by two μ-η^2:η^1 acetates and one *syn-syn* acetate. The Gd1···Gd1A distance is 4.0552(2) Å, and the Gd−O−Gd angle is 110.00(15)° (Gd1−O1−Gd1A) and 112.62(15)° (Gd1−O6−Gd1A), respectively. There exist intramolecular $O_{methanol}$−H···$O_{carboxylate}$ hydrogen bonding interactions (O7A−H···O4B). The Gd−Gd−Gd angle is 142.58(8)°. The smallest interchain Gd···Gd separation is 8.373 Å. The adjacent chains are structurally well isolated due to the absence of no significant interchain hydrogen bonding interactions. It should be noted that complex **3** is isostructural with the previously reported 1D dysprosium(III) chain structure.[9]

dx.doi.org/10.1021/ic2018314 | *Inorg. Chem.* 2012, 51, 405−413

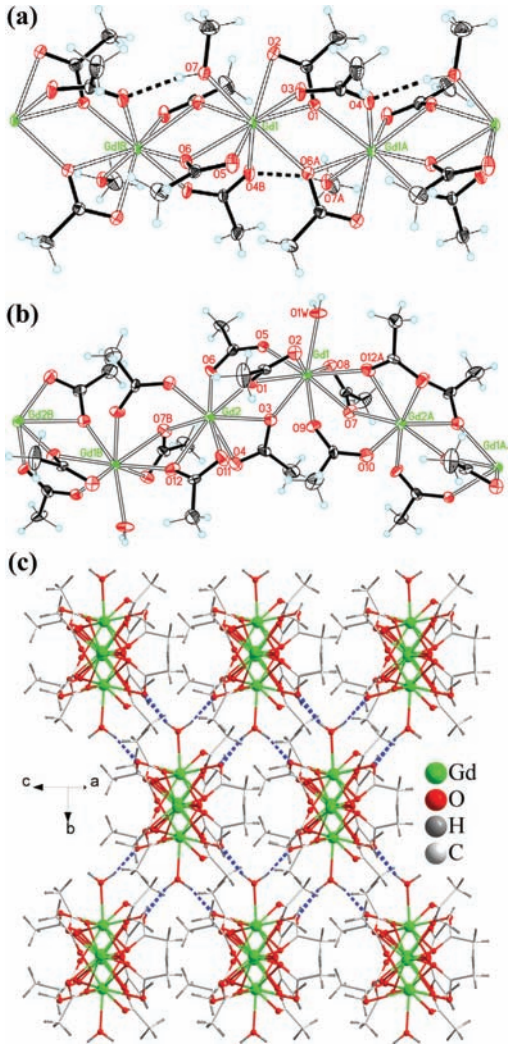

Figure 2. The 1D chain structures of **3** (a) and **4** (b) with ellipsoids at the 30% probability level. (c) The 3D hydrogen-bonded network in **4**. Color codes: Gd, vivid green; C, light gray; O, red; H, gray; hydrogen bond, blue.

Complex **4** crystallizes in the monoclinic space group *Cc*. Similar to that of **3**, **4** has also a 1D coordination chain structure (Figure 2b). The asymmetric unit contains two Gd^{III} ions and six carboxylate ligands as well as one monodentate aqua ligand. Four of the acetato ligands are bonded in the μ-η^2:η^1 fashion; the other two acetato ligands are in the *syn-syn* μ-η^1:η^1 mode. The nine-coordinate (capped square-antiprismatic) Gd1 and the eight-coordinate (square-antiprismatic) Gd2 ions are bridged by two μ-η^2:η^1 acetates and one *syn-syn* acetate. In the zigzag chain, Gd1 is located at the vertex; the Gd1···Gd2 distance is 4.0273(14) Å (Gd2, on one side of Gd1) and 4.0340(14) Å (Gd2, on another side of Gd1), respectively. The Gd1−O1−Gd2, Gd1−O3−Gd2, Gd1−O7−Gd2 and Gd1−O12−Gd2 angles are 112.4(4)°, 106.5(4)°, 108.4(4)° and 109.8(4)°, respectively. Notably, both the Gd−O−Gd angle and Gd···Gd distance in **4** are smaller than those in **3**. There are two kinds of Gd−Gd−Gd angles, 128.62(8)° and 175.28(3)°, resulting in the 1D zigzag chain, quite different from that in **3**. The smallest interchain Gd···Gd separation is 6.461 Å. It should be noted that there is no intrachain hydrogen bonding interaction. However, the 1D coordination chains are extended into a 3D supramolecular architecture by the interchain O_{water}−H···$O_{carboxylate}$ hydrogen bonding interactions (Figure 2c).

Magnetic Properties. The static magnetic moment of polycrystalline sample of **1** was measured in the temperature range 2 to 300 K at 500 G (Figure 3a). The room-temperature χT value of 15.79 cm^3 K mol^{-1} for **1** is in good agreement with the spin-only value of 15.75 cm^3 K mol^{-1} expected for two uncoupled Gd^{3+} ions (g = 2). As the temperature decreases, χT stays essentially constant until at approximately 30 K, the value increases sharply to a maximum value of 18.09 cm^3 K mol^{-1} at 2 K. The increase of χT at low temperature indicates the presence of intramolecular ferromagnetic Gd(III)···Gd(III) interactions.

The variable temperature susceptibility data obey the Curie−Weiss law (eq 1) with C = 15.79(6) cm^3 K mol^{-1}, θ = 0.18(1) K (shown in Figure 3a). The susceptibility data was further analyzed by an isotropic exchange expression derived from the Hamiltonian (eq 2) for **1**, where $S_1 = S_2 = 7/2$, the best fitting results give J = 0.04(1) cm^{-1}, g = 2.00(1), and zJ = 0 with $R = 2.0 \times 10^{-6}$ ($R = [\sum(\chi_{obs}T - \chi_{fit}T)^2/\sum(\chi_{obs}T)^2]^{1/2}$), where zJ is the intermolecular interaction as a correction by the molecule field theory. The solid lines represent the fitted results.

$$\chi = C/(T - \theta) \tag{1}$$

$$\hat{H} = -J\hat{S}_1\cdot\hat{S}_2 + g\mu_B\hat{S}_zH \tag{2}$$

The presence of ferromagnetic Gd(III)···Gd(III) interactions is further supported by magnetization measurements (blue circles, Figure 3b). Under high magnetic field (70 kG) and low temperature (2 K), M reaches a saturation value of 14.04 $N\beta$. The red solid line corresponds to the Brillouin function for the parameters obtained from the static susceptibility data. The calculated curve matches very well the experimental data. In addition, the red line is sandwiched in between the two dashed lines that correspond to (A) an S = 7 state and to (B) two uncoupled Gd centers, which confirms the occurrence of a weak ferromagnetic interaction between the two gadolinium ions.

The χT curve of **2** (Figure 3c) is similar to that of **1**. At room temperature, the χT value of 31.52 cm^3 K mol^{-1} is in agreement with the expected value (7.88 cm^3 K mol^{-1} × 4). χT remains constant to about 35 K before increasing to a maximum of 37.10 cm^3 K mol^{-1} at 1.8 K. This behavior can be attributed to the intramolecular ferromagnetic exchange. The variable temperature susceptibility data obey the Curie−Weiss law with C = 31.53(3) cm^3 K mol^{-1}, θ = 0.23(2) K (shown in Figure 3c). The susceptibility data was further analyzed using MAGPACK,[12] and the Hamiltonian,

$$\hat{H} = -J_1(\hat{S}_{Gd1}\cdot\hat{S}_{Gd2} + \hat{S}_{Gd1A}\cdot\hat{S}_{Gd2A}) - J_2\hat{S}_{Gd2}\cdot\hat{S}_{Gd2A} + g\mu_B\hat{S}_zH \tag{3}$$

was got by the coupling pathway as shown in the top of Figure 3c.

The distance between Gd1 and Gd2A (Gd1A and Gd2) is 7.086 Å; for convenience of data analysis, we set the exchange interactions J equal to zero for the large distance and J_1 and J_2 have the same value. The red solid line in Figure 3c represents the simulation result, giving $J_1 = J_2$ = 0.02(1) cm^{-1} and g = 2.00(1) with $R = 3.0\times 10^{-6}$. The positive parameters show that intramolecular Gd1···Gd2, Gd2···Gd2A, Gd2A···Gd1A interactions in **2** are weakly ferromagnetic, which is further

dx.doi.org/10.1021/ic2018314 | *Inorg. Chem.* 2012, 51, 405−413

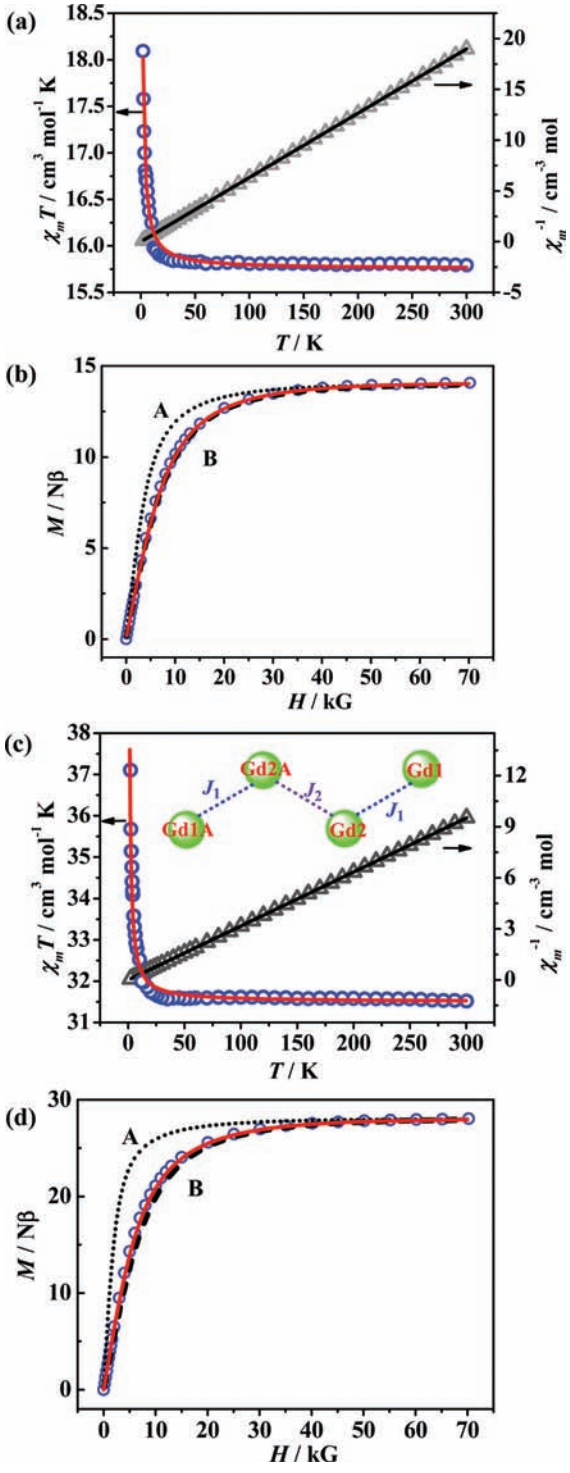

Figure 3. Temperature dependence of the χT and the inverse molecular susceptibility plots at 500 G for **1** (a) and **2** (c); the red line represents the best fitted result. Magnetization versus field of **1** (b) and **2** (d) at 2 K. The red solid line corresponds to the Brillouin function for the parameters obtained from the static susceptibility data (see text), and the dashed lines represent the Brillouin function for (A) an S = 7 (**1**)/14 (**2**) state and (B) two/four uncoupled Gd centers. Magnetic coupling scheme of **2** (top of c).

supported by the experimental M versus H data and the calculated results shown in Figure 3d.

The static magnetic moment of polycrystalline samples of **3** was measured using a SQUID magnetometer in the temperature range 2 to 300 K at 500 G (Figure 4a). The room temperature χT value of 7.84 cm^3 K mol^{-1} for **3** is in good agreement with the spin-only (g = 2) value of 7.88 cm^3 K

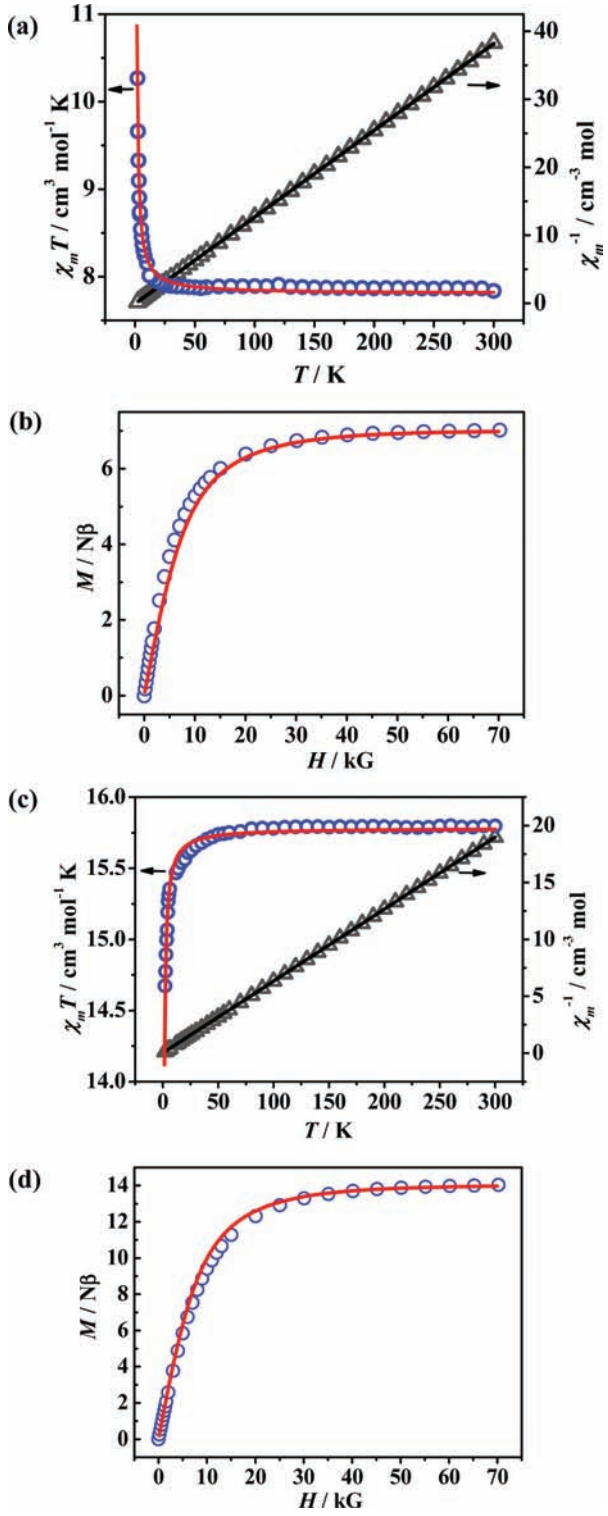

Figure 4. Temperature dependence of the χT and the inverse molecular susceptibility plots at 500 G for **3** (a) and **4** (c); the red lines represent the fitted results. Magnetization (M) versus field (H) of **3** (b) and **4** (d) at applied fields of 0−70 kG at 2 K; the solid lines are the Brillouin function for one (**3**) and two (**4**) magnetically isolated S = 7/2 with g = 2.0.

dx.doi.org/10.1021/ic2018314 | Inorg. Chem. 2012, 51, 405−413

Table 2. Selected Magnetostructural Data of Gadolinium(III) Complexes

complex[a]	Gd···Gd/Å	Gd−O−Gd/deg	J^b/cm^{-1}	bridge	ref
$[Gd_2(OAc)_6(H_2O)_4]\cdot 4H_2O$	4.206	115.5	0.06	A	14a
$[Gd_2(Hsal)_6(H_2O)_2]$	4.250	116.118	0.05	A	14b
$[Gd_2(mal)_3(H_2O)_6]_n$	4.276	116.71	0.048	A	14c
$[Gd(Hcit)(H_2O)_2]_n\cdot nH_2O$	4.321	118.49	0.039	A	15a
$[Gd_2(OAc)_6(H_2O)_4]\cdot 2H_2O$	4.159	115.47	0.031	A	15b
$[Gd_2(tpac)_6(H_2O)_4]$	4.126	112.5	−0.012	A	15c
$[Gd_2(pac)_6(H_2O)_4]$	4.122	113.16	−0.032	A	15c
$[Gd_2(OAc)_2(Ph_2acac)_4(MeOH)_2]$	4.128	113.65	0.038	A	**1**
$[Gd_4(OAc)_4(acac)_8(H_2O)_4]$	4.271/4.334	114.45/117.73	0.024	A	**2**
$[Gd(H_2sal)(Hsal)(sal)(H_2O)]_n$	4.187	111.85/114.29	0.037	B	16a
$[Gd(mta)(H_2O)]_n\cdot nH_2O$	4.065	110/112.3	0.026	B	16b
$[Gd_2(succinate)_3(H_2O)_2]_n\cdot 0.5nH_2O$	4.059	109.96/112.24	0.019	B	16c
$[Gd(OAc)_3(MeOH)]_n$	4.055	110/112.62	0.033	B	**3**
$[Gd(OAc)_3(H_2O)]_n$	4.027/4.034	106.5/108.4	−0.011	B	**4**

[a]Abbreviations used: OAc = acetate, H_2sal = salicylic acid, H_2mal =1,3-propanedioic acid, H_4cit = citric acid, tpac =3-thiopheneacetate, pac = pentanoate, H_3mta = methanetriacetic acid. [b]The spin Hamiltonian is defined as $\hat{H} = -J\,\hat{S}_A\cdot\hat{S}_B$.

mol^{-1}. As the temperature decreases, χT stays essentially constant to about 30 K before increasing to a maximum of 10.27 cm^3 K mol^{-1} at 2 K, indicating the presence of intramolecular ferromagnetic interactions between Gd^{3+} centers.

The χT curve of **4** is shown in Figure 4c; at room temperature, the χT value of 15.80 cm^3 K mol^{-1} is in good agreement with the expected value (7.88 cm^3 K mol^{-1} per Gd(III) unit × 2). χT remains constant to about 35 K, after which it decreases abruptly to a minimum value of 14.67 cm^3 K mol^{-1} at 2.0 K. This plot is indicative of the occurrence of a weak antiferromagnetic interaction between the gadolinium ions in **4**.

The susceptibility data obey the Curie−Weiss law with C = 7.85(6) cm^3 K mol^{-1}, θ = 0.34(2) K for **3** (inset of Figure 4a) and C = 15.81(4) cm^3 K mol^{-1}, θ = −0.22(1) K for **4** (inset of Figure 4c), respectively.

Owing to structural findings, we consider in what follows the chain with nearest neighbor exchange interactions described by the following spin Hamiltonian:[13]

$$H = -J\sum S_{2i}S_{2i+1} \tag{4}$$

where J stands for the exchange constant, and the S = 7/2. For complex **3**, the best fitting results give g = 1.99(1), J = 0.03(1) cm^{-1}, and zJ = 0 with $R = 2.0\times10^{-6}$, where zJ is the interchain interaction as a correction by the molecular field theory. This result indicates that the ferromagnetic coupling between adjacent Gd^{3+} ions within the chain is very weak and there is no remarkable magnetic interaction between chains. In **4**, for convenience of data analysis, we set the nearest neighbor exchange interactions J to have the same value, and the best fitting results give g = 2.00(1), J = −0.01(1) cm^{-1}, and zJ = 0 with $R = 5.0\times10^{-6}$.

Figures 4b and 4d show the M versus H plot of **3** and **4**, respectively. Under high magnetic fields at low temperature, the magnetization data reach to the saturated value of 7.02 $N\beta$ for **3** and 14.04 $N\beta$ for **4**. In Figure 4b, the experimental magnetization curve is above the red line that presents the Brillouin function for magnetically uncoupled gadolinium ions with S = 7/2 and g = 2.0, confirming again the ferromagnetic coupling interaction between the Gd(III) ions in complex **3**. For **4**, the lower experimental magnetization curve supports the antiferromagnetic correlation between Gd(III) ions.

Complexes **1** and **2** have the same exchange pathway (type A) between the Gd(III) ions. The bridges between the Gd(III) ions in **3** and **4** are the same: two μ-oxo acetates and one *syn-syn* acetate (type B). However, the nature of the weak magnetic coupling of **3** (ferromagnetic) and **4** (antiferromagnetic) is different. The values of the magnetic coupling can be compared with those observed for other magnetostructurally characterized carboxylate-containing Gd(III) complexes. The available data are summarized in Table 2.[14] It seems that there exists a connection between the Gd−O−Gd angle (or the intramolecular Gd···Gd distance) and the magnetic exchange: a ferromagnetic interaction is favored when the Gd−O−Gd angle and Gd···Gd distance are large; and the Gd−O−Gd angle and Gd···Gd distance of **1** and **2** (ferromagnetic) are larger than those of $[Gd_2(tpac)_6(H_2O)_4]$ and $[Gd_2(pac)_6(H_2O)_4]$[15c] (antiferromagnetic).[14,15] There are very few complexes containing the same bridges as **3** and **4**, and all are weakly ferromagnetic,[16] in which the Gd···Gd distances vary from 4.059 to 4.187 Å, and Gd−O−Gd angles vary from 109.96 to 114.29°, larger than those of **3** and **4**.

There is weak Gd(III)···Gd(III) magnetic coupling in complexes **1**−**4**; combined with the different structure and M_W/N_{Gd} ratio, this urges us to evaluate the MCE.

The MCE can be described by the Maxwell relation as the following:

$$\Delta S_m(T)_{\Delta H} = \int [\partial M(T, H)/\partial T]_H \, dH \tag{5}$$

According to eq 5,[1−5] we can obtain the $-\Delta S_m$ of **1** from the experimental magnetization data (Figure 5a), and the curves of $-\Delta S_m$ (circles) are depicted in Figures 5c and S1 in the Supporting Information. The changes of magnetic entropy give the maximum value of 23.7 J K^{-1} kg^{-1} (expected maximum entropy value is 24.9 J K^{-1} kg^{-1} calculated as $2R\ln(2s+1)$) for a field change ΔH = 70 kG at approximately 2.4 K.

The expected maximum entropy change of **2** is 40.0 J K^{-1} kg^{-1}, calculated as $4R\ln(2S+1)$ for four uncoupled Gd^{III} ions, which is close to the $-\Delta S_m$ obtained from the magnetization data (Figure 5b), giving the maximum value of 37.7 J K^{-1} kg^{-1} for a field change ΔH = 70 kG at approximately 2.4 K (circles). In addition, it is worth noting that $-\Delta S_m$ is already up to 30.6 J K^{-1} kg^{-1} at a field change ΔH = 30 kG at 2.0 K.

dx.doi.org/10.1021/ic2018314 | Inorg. Chem. 2012, 51, 405−413

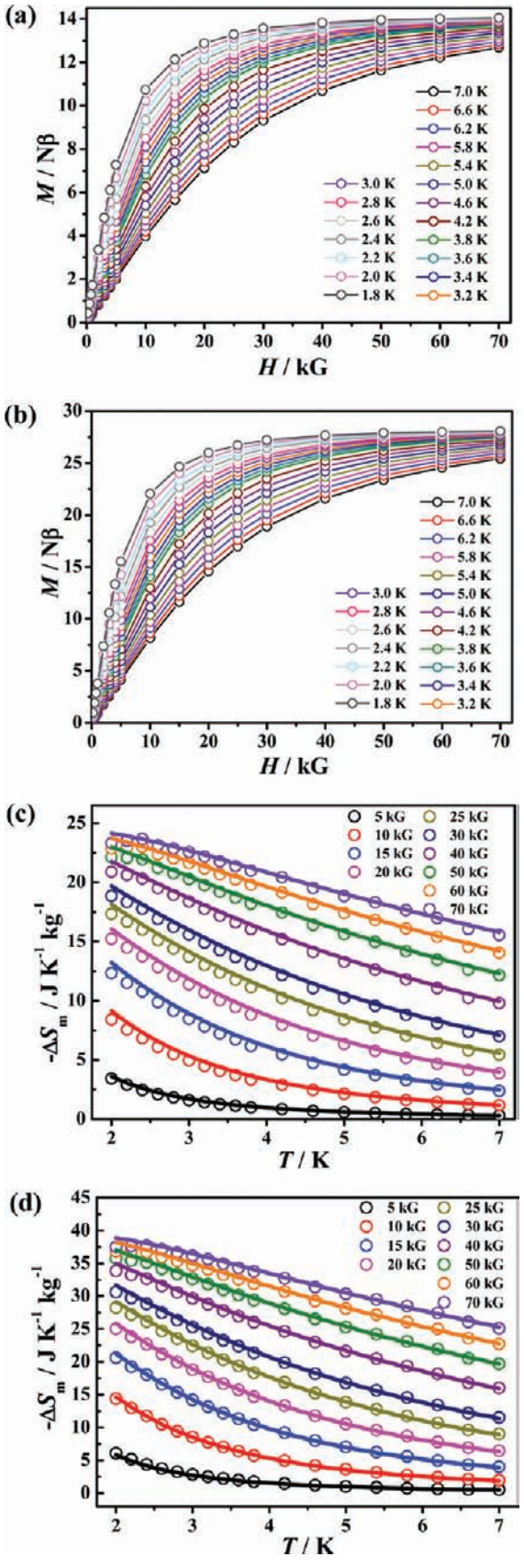

Figure 5. Magnetization versus applied field of **1** (a) and **2** (b) at T = 1.8−7.0 K and H = 0.25−70 kG. Experimental $-\Delta S_m$ obtained from magnetization data of **1** (c) and **2** (d) at various fields and temperatures (circles) and the simulated curve of $-\Delta S_m$ (solid lines).

For complex **3** (see Figures 6a, 6c and S3 in the Supporting Information), it can be seen that the $-\Delta S_m$ (see experimental magnetization data in Figure 6a) value increases gradually with the increasing ΔH and the decreasing temperature, reaching a maximum value of 45.0 J K^{-1} kg^{-1} (expected maximum entropy value per mole is 47.2 J K^{-1} kg^{-1} calculated as R ln(2s+1) for one isolated Gd^{III} ion) for a field change ΔH = 70 kG at approximately 1.8 K. For complex **4** (see Figures 6b, 6d and S4 in the Supporting Information), the expected maximum entropy change is 50.4 J K^{-1} kg^{-1}, calculated as 2R ln(2s+1) for two uncoupled Gd^{III} ions. The $-\Delta S_m$ obtained from the magnetization data (Figure 6b) gives the maximum value of 47.7 J K^{-1} kg^{-1} for a field change ΔH = 70 kG at approximately 1.8 K (circles). The $-\Delta S_m$ values of **1**−**4** can be compared with those observed for other selected 3d/3d-4f/4f complexes. The available data are listed in Table 3.

Because of the lower M_W/N_{Gd} ratio than **3**, the maximum MCE value of complex **4** is larger than **3**, which is larger than all of the reported cases. Additionally, it is worth mentioning that the $-\Delta S_m$ value of complex **3** is gets larger than that of **4** with the decreasing ΔH; for example, the $-\Delta S_m$ value is 6.0 J K^{-1} kg^{-1} for **3** and 4.2 J K^{-1} kg^{-1} for **4** at 1.8 K with ΔH = 4.0 kG (Figures S3 and S4 in the Supporting Information), which should be attributed to the ferromagnetic coupling in **3**. The dominant ferromagnetic coupling makes a large $-\Delta S_m$ easily accessible under a limited change in temperature and/or field. In other words, complex **3** has wider temperature and/or field scope of application in refrigeration.

If we know the electronic configuration and the partition function Z of one system, the magnetic entropy can be determined by the equation

$$S = R \ln Z + RT(\partial \ln Z/\partial T) \quad (6)$$

[17]where the partition function Z was defined as $Z = \sum e^{-\varepsilon_i/kT}$. Thus, the entropy can be derived as

$$S/R = \ln \sum e^{-\varepsilon_i/kT} + \frac{1}{kT}\frac{\sum \varepsilon_i e^{-\varepsilon_i/kT}}{\sum e^{-\varepsilon_i/kT}} \quad (7)$$

The energy levels can be calculated by the Hamiltonian:

$$\hat{H} = -\sum J\hat{S}_1\cdot\hat{S}_2 + g\beta\hat{S}_z H - zJ\langle S_z\rangle\hat{S}_z \quad (8)$$

Thus, the magnetic entropy change, $\Delta S_m(T)$, can be simulated from the statistical thermodynamics on entropy based on eqs 6−8. Detailed introduction has been referenced in the Supporting Information.

The simulated results (solid lines) are shown in Figures 5c (**1**), 5d (**2**), 6c (**3**) and 6d (**4**) and Figures S1−S4 in the Supporting Information, which are quite well in accordance with the magnetic entropy change $\Delta S_m(T)$ as indirectly obtained from magnetization data (circles), suggesting that it would be a promising method for predicting the MCE of molecule-based magnets.

CONCLUSION

In this study, two polynuclear clusters and two one-dimensional Gd(III) chains based on gadolinium acetate were characterized. Magnetic studies reveal that weak ferromagnetic interactions occur in **1**, **2** and **3** due to the presence of large Gd−O−Gd angles (Gd···Gd distances), and antiferromagnetic interaction in **4** when the Gd−O−Gd angle is relatively smaller. These complexes provide new magnetostructural data of Gd(III)

dx.doi.org/10.1021/ic2018314 | Inorg. Chem. 2012, 51, 405−413

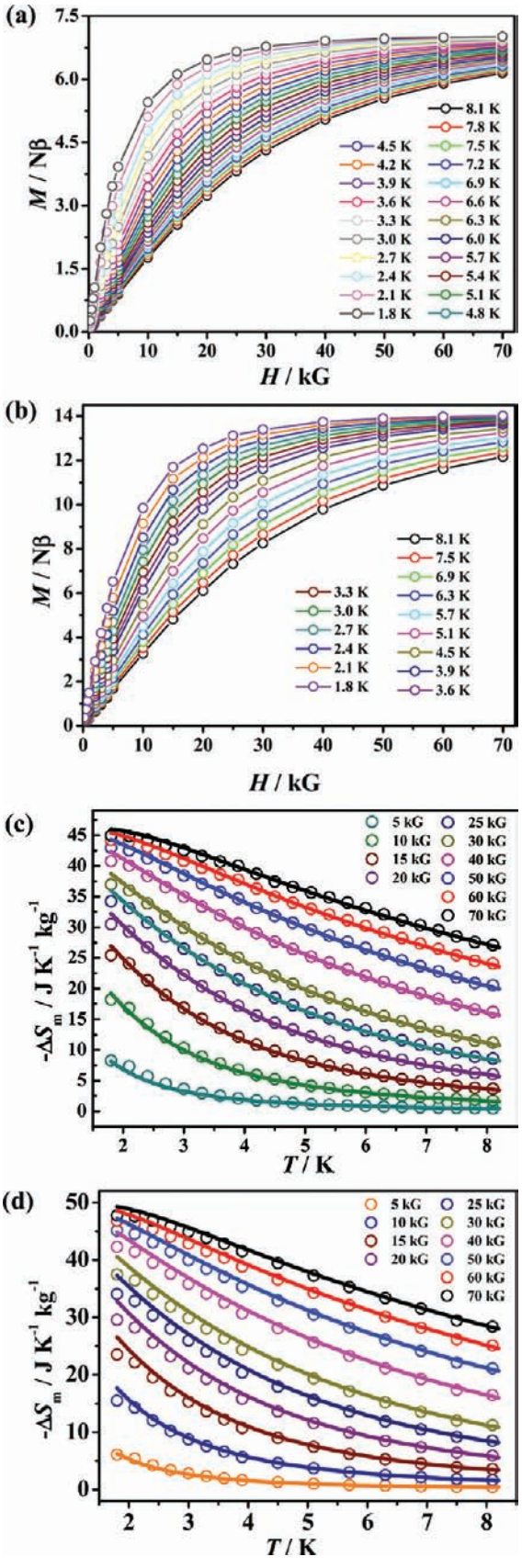

Figure 6. Magnetization versus applied field of **3** (a) and **4** (b) at T = 1.8−8.1 K and H = 0.25−70 kG. Experimental $-\Delta S_m$ (circles) obtained from magnetization data of **3** (c) and **4** (d) at various fields and temperatures and the simulated curve of $-\Delta S_m$ (lines).

Table 3. Selected $-\Delta S_m$ Data of 3d/3d-4f/4f Complexes

complex	$-\Delta S_m$/J K^{-1} kg^{-1}	ref
$[Fe_{14}O_6(ta)_6(OMe)_{18}Cl_6]$	20.3 (70 kG)	2c
$\{Mn^{III}_6Mn^{II}_4\}$	13.0 (70 kG)	2b
$\{Mn^{III}_6Mn^{II}_8\}$	25 (70 kG)	3a
$\{Mn^{III}_4Gd^{III}_4\}$	19.0 (70 kG)	3b
$\{Co^{II}_4Gd^{III}_6\}$	22.3 (70 kG)	6a
$\{Ni_6Gd_6P_6\}$	26.5 (70 kG)	6b
$\{Cu^{II}_5Gd^{III}_4\}$	31 (90 kG)	4a
$[Gd_2(fum)_3(H_2O)_4]\cdot 3H_2O$	20.7 (50 kG)	8a
$\{Gd_7\}$	23 (70 kG)	8b
$[Gd_2(OAc)_2(Ph_2acac)_4(MeOH)_2]$	23.7 (70 kG)	**1**
$[Gd_4(OAc)_4(acac)_8(H_2O)_4]$	37.7 (70 kG)	**2**
$[Gd_2(OAc)_6(H_2O)_4]\cdot 4H_2O$	41.6 (70 kG)	4b
$[Gd(OAc)_3(MeOH)]_n$	45.0 (70 kG)	**3**
$[Gd(OAc)_3(H_2O)_{0.5}]_n$	47.7 (70 kG)	**4**

complexes. All complexes display large MCE. The lower M_W/N_{Gd} ratio in the gadolinium acetate system, the larger MCE they display. Moreover, the statistical thermodynamics on entropy was successfully applied to simulate the MCE values of the four complexes. The results are quite in agreement with those obtained from experimental data, suggesting that it would be a promising method for predicting the MCE of molecule-based magnets. Complex **4** has the highest magnetic density and exhibits the largest MCE (47.7 J K^{-1} kg^{-1}) among the four gadolinium acetate derivatives, which is also highest among the recently reported MCE values, while complex **3** has wider temperature and/or field scope of application in refrigeration for the dominant ferromagnetic coupling.

■ ASSOCIATED CONTENT

Supporting Information

Method for the simulation of MCE values by the statistical thermodynamics on entropy, the curves of $-\Delta S_m$ at low fields and spin energy level of **2** simulated by MAGPACK. This material is available free of charge via the Internet at http://pubs.acs.org.

■ AUTHOR INFORMATION

Corresponding Author

*E-mail: tongml@mail.sysu.edu.cn.

■ ACKNOWLEDGMENTS

This work was supported by the NSFC (Grants 91122032, 50872157, 90922009 and 20821001) and the "973 Project" (2012CB821704).

■ REFERENCES

(1) (a) Warburg, E. *Ann. Phys.* **1881**, *249*, 141. (b) Debye, P. *Ann. Phys.* **1926**, *386*, 1154. (c) Giauque, W. F. *J. Am. Chem. Soc.* **1927**, *49*, 1864. (d) Pecharsky, V. K.; Gschneidner, K. A. Jr. *J. Magn. Magn. Mater.* **1999**, *200*, 44. (e) Gschneidner, K. A. Jr.; Pecharsky, V. K. *Int. J. Refrig.* **2008**, *31*, 945.

(2) (a) Evangelisti, M.; Candini, A.; Ghirri, A.; Affronte, M.; Brechin, E. K.; McInnes, E. J. L. *Appl. Phys. Lett.* **2005**, *87*, 072504. (b) Manoli, M.; Johnstone, R. D. L.; Parsons, S.; Murrie, M.; Affronte, M.; Evangelisti, M.; Brechin, E. K. *Angew. Chem., Int. Ed.* **2007**, *119*, 4440. (c) Shaw, R.; Laye, R. H.; Jones, L. F.; Low, D. M.; Talbot-Eeckelaers, C.; Wei, Q.; Milios, C. J.; Teat, S.; Helliwell, M.; Raftery, J.; Evangelisti, M.; Affronte, M.; Collison, D.; Brechin, E. K.; McInnes, E. J. L. *Inorg. Chem.* **2007**, *46*, 4968.

(3) (a) Manoli, M.; Collins, A.; Parsons, S.; Candini, A.; Evangelisti, M.; Brechin, E. K. *J. Am. Chem. Soc.* **2008**, *130*, 11129. (b) Karotsis, G.; Evangelisti, M.; Dalgarno, S. J.; Brechin, E. K. *Angew. Chem., Int. Ed.* **2009**, *48*, 9928−9931. (c) Karotsis, G.; Kennedy, S.; Teat, S. J.; Beavers, C. M.; Fowler, D. A.; Morales, J. J.; Evangelisti, M.; Dalgarno, S. J.; Brechin, E. K. *J. Am. Chem. Soc.* **2010**, *132*, 12983. (d) Evangelisti, M.; Brechin, E. K. *Dalton Trans.* **2010**, *39*, 4672.

(4) (a) Langley, S. K.; Chilton, N. F.; Moubaraki, B.; Hooper, T.; Brechin, E. K.; Evangelisti, M.; Murray, K. S. *Chem. Sci.* **2011**, *2*, 1166. (b) Evangelisti, M.; Roubeau, O.; Palacios, E.; Camín, A.; Hooper, T. N.; Brechin, E. K.; Alonso, J. J. *Angew. Chem., Int. Ed.* **2011**, *50*, 6606.

(5) (a) Zhang, X. X.; Wei, H. L.; Zhang, Z. Q.; Zhang, L. *Phys. Rev. Lett.* **2001**, *87*, 157203. (b) Evangelisti, M.; Luis, F.; de Jongh, L. J.; Affronte, M. *J. Mater. Chem.* **2006**, *16*, 2534. (c) Nayak, S.; Evangelisti, M.; Powell, A. K.; Reedijk, J. *Chem.—Eur. J.* **2010**, *16*, 12865. (d) Liu, J.-L.; Leng, J.-D.; Lin, Z.; Tong, M.-L. *Chem. Asian J.* **2011**, *6*, 1007.

(6) (a) Zheng, Y.-Z.; Evangelisti, M.; Winpenny, R. E. P. *Chem. Sci.* **2011**, *2*, 99. (b) Zheng, Y.-Z.; Evangelisti, M.; Winpenny, R. E. P. *Angew. Chem., Int. Ed.* **2011**, *50*, 3692.

(7) (a) Shen, B. G.; Sun, J. R.; Hu, F. X.; Zhang, H. W.; Cheng, Z. H. *Adv. Mater.* **2009**, *21*, 4545. (b) Spichkin, Y. I.; Zvezdin, A. K.; Gubin, S. P.; Mischenko, A. S.; Tishin, A. M. *J. Phys. D* **2001**, *34*, 1162. (c) Gschneidner, K. A. Jr.; Pecharsky, V. K.; Tsokol, A. O. *Rep. Prog. Phys.* **2005**, *68*, 1479. (d) Zimm, C.; Jastrab, A.; Sternberg, A.; Pecharsky, V. K.; Gschneidner, K. A. Jr.; Osborne, M.; Anderson, I. *Adv. Cryog. Eng.* **1998**, *43*, 1759.

(8) (a) Sedláková, L.; Hankoa, J.; Orendáčová, A.; Orendáč, M.; Zhou, C.-L.; Zhu, W.-H.; Wang, B.-W.; Wang, Z.-M.; Gao, S. *J. Alloys Compd.* **2009**, *487*, 425. (b) Sharples, J. W.; Zheng, Y.-Z.; Tuna, F.; McInnes, E. J. L.; Collison, D. *Chem. Commun.* **2011**, *47*, 7650.

(9) Zheng, Y.-Z.; Lan, Y.; Wernsdorfer, W.; Anson, C. E.; Powell, A. K. *Chem.—Eur. J.* **2009**, *15*, 12566.

(10) (a) Chen, X.-Y.; Yang, X.; Holliday, B. J. *Inorg. Chem.* **2010**, *49*, 2583. (b) Petit, S.; Baril-Robert, F.; Pilet, G.; Reber, C.; Luneau, D. *Dalton Trans.* **2009**, 6809.

(11) Wu, Y.; Morton, S.; Kong, X.; Nichola, G. S.; Zheng, Z. *Dalton Trans.* **2011**, *40*, 1041.

(12) Borrás-Almenar, J. J.; Clemente-Juan, J. M.; Coronado, E.; Tsukerblat, B. S. *Inorg. Chem.* **1999**, *38*, 6081.

(13) (a) Kahn, O. *Molecular Magnetism*; VCH Publishers: New York, 1993. (b) Fisher, M. E. *Am. J. Phys.* **1964**, *32*, 343.

(14) (a) Hatscher, S. T.; Urland, W. *Angew. Chem., Int. Ed.* **2003**, *42*, 2862. (b) Costes, J.-P.; Clemente-Juan, J. M.; Dahan, F.; Nicodème, F.; Verelst, M. *Angew. Chem., Int. Ed.* **2002**, *41*, 323. (c) Hernández-Molina, M.; Ruiz-Pérez, C.; López, T.; Lloret, F.; Julve, M. *Inorg. Chem.* **2003**, *42*, 5456.

(15) (a) Baggio, R.; Calvo, R.; Garland, M. T.; Peña, O.; Perec, M.; Rizzi, A. *Inorg. Chem.* **2005**, *44*, 8979. (b) Cañadillas-Delgado, L.; Fabelo, O.; Cano, J.; Pasán, J.; Delgado, F. S.; Lloret, F.; Julve, M.; Ruiz-Pérez, C. *CrystEngComm* **2009**, *11*, 2131. (c) Cañadillas-Delgado, L.; Fabelo, O.; Pasán, J.; Delgado, F. S.; Lloret, F.; Julveb, M.; Ruiz-Pérez, C. *Dalton Trans.* **2010**, *39*, 7286.

(16) (a) Costes, J.-P.; Clemente-Juan, J. M.; Dahan, F.; Nicodème, F. *Dalton Trans.* **2003**, 1272. (b) Cañadillas-Delgado, L.; Martín, T.; Fabelo, O.; Pasán, J.; Delgado, F. S.; Lloret, F.; Julve, M.; Ruiz-Pérez, C. *Chem.—Eur. J.* **2010**, *16*, 4037. (c) Manna, S. C.; Zangrando, E.; Bencini, A.; Benelli, C.; Chaudhuri, N. R. *Inorg. Chem.* **2006**, *45*, 9114.

(17) Carlin, R. L. *Magnetochemistry*; Springer: Berlin, 1986.